Dysregulation of ferroptosis may involve in the development of non-small cell lung cancer in Xuanwei area

Zhang Yang (zhang.yang@dbmr.unibe.ch)
Inselspital Universitatsspital Bern

Guangjian Li
Yunnan Cancer Hospital

Jiapeng Yang
Yunnan Cancer Hospital

Guangqiang Zhao
Yunnan Cancer Hospital

Zhenghai Shen
Yunnan Cancer Hospital

Kaiyun Yang
Yunnan Cancer Hospital

Linwei Tian
Shenzhen Institute of Hong Kong Univertisy

Qinghua Zhou
Sichuan University West China Hospital

Ren-Wang Peng
Inselspital Universitatsspital Bern

Ying Chen
Yunnan Cancer Hospital

Research

Keywords: Xuanwei, lung cancer, thioredoxin, haptoglobin, ferroptosis

Posted Date: August 2nd, 2020

DOI: https://doi.org/10.21203/rs.3.rs-49019/v1

Abstract

Background

The Xuanwei area of Yunnan Province, China is one of the regions with the highest incidence of lung cancer in the world. Local residents use bituminous coal as fuel for cooking and heating, which causes serious indoor air pollution. After the local government carried out furnace and stove reform work, the high incidence of lung cancer in residents continued. We herein wonder if there are specific mechanisms at protein level for the development of lung cancer in the area.

Methods

We investigated the changes of protein profiling in tumor of the patients from Xuanwei area. Tandem Mass Tag (TMT) were employed to screen the differential proteins between carcinoma and para-carcinoma tissues.

Results

We identified a total of 422 differentially-expressed proteins, among which 162 proteins were significantly upregulated and 260 were downregulated compared to para-carcinoma tissues. Many of the differentially-expressed proteins were related to ECM-receptor interaction, focal adhesion, PI3K/AKT pathway and ferroptosis. Further experiments on the two differential proteins, TXN2 and HP, showed that the change of their expressions could make the lung cancer cell lines more resistant to erastin or RSL-induced ferroptosis *in vitro*, and promote the growth of tumor in nude mice.

Conclusion

This study revealed that aberrant regulation of ferroptosis may involve in the development of lung cancer in Xuanwei area.

Introduction

The number of deaths due to cancer accounts for about 12% of the total deaths each year worldwide, and there are more than 1 million new cases of cancer each year (1). Lung cancer has become the leading cause of cancer deaths in humans. Xuanwei area in Yunnan province, including Xuanwei, Fuyuan, Qilin and Zhanyi Counties (E 103°35'30"-104°49'48", N 25°02'38"-26°44'50"), located in southwestern China, has a population of about 3.1 million, and is one of the regions with the highest incidence of lung cancer in the world. Especially in Xuanwei County, the incidence of lung cancer among non-smokers is 400 / 100,000, which is 20 times higher than the national average (2, 3). Previous research has linked this excess lung cancer rate with the domestic combustion of “smoky coal”, especially burning the coals in

unvented households (4, 5). The term smoky coal refers to the locally available Late Permian bituminous coal (6), which releases a large amounts of visible smoke upon combustion. The coal is the primary fuel source for cooking and heating for residents in Xuanwei area and is available from many coal mines throughout the region. Research thus far has indicated that the smoky coal emits high levels of polycyclic aromatic hydrocarbons (PAHs) and contains high concentrations of fine-grained crystalline quartz, both of them are classified by the International Agency for Research on Cancer (IARC) as carcinogenic to humans (7, 8). The Yunnan Provincial Government has carried out furnace and stove reform work in Xuanwei area, hoping to reduce the incidence of lung cancer by reducing indoor coal-burning air pollution. However, the results of the Third National Sampling Survey of Cause of Death showed that the lung cancer mortality rate in the whole Xuanwei area increased most significantly nationwide (9). Therefore, there could be other more important carcinogens.

Relationship between the high lung cancer incidence in Xuanwei residents and environmental pollution has been a hot topic in the field of environmental sciences. The mean concentrations of V, Cd, Cr, Cu, Mn, Co, Ni, Pb, As and Zn were all higher than the background values in Yunnan soil, indicating that the street dusts of Xuanwei city have been heavily polluted by those metals. The 5 carcinogenic metals, including Cd, Cr, Ni, Cr and As, had a potential risk of carcinogenicity in human after exposed to the dusts, and Cr was the major toxic element to the local children's health (10). The roles of some metal elements, especially heavy metal elements, are partially known in carcinogenesis of lung cancer. The toxic effect of Pb on the lung was associated with significant increases in NF-κB and AHR levels which was associated with increases in downstream targets genes, iNOS and CYP1A1 (11). Another study reported that Cr(VI) could induce DNA methylation and silencing of the gpt transgene in G12 Chinese hamster lung cells (12). Moreover, lower Ti but higher levels of miR-24-3p and miR-28-5p were shown in tumor than normal tissues of lung squamous cell carcinoma patients (13). Some other studies have found the association between the high lung cancer incidence and the contamination of metal elements in Xuanwei area (10, 14). A recent study showed that the average concentrations of heavy metals in road dust were higher than their background values, and higher concentrations of heavy metals were found in the magnetic fractions than in the non-magnetic fractions in the region (15).

Thus, we hypothesized that the geological composition of the Xuanwei area may have the development of lung cancer in this area special molecular mechanisms. Furthermore, we would analyze the protein profiling changes of the lung cancer tissues form the patients of Xuanwei area, providing more insights to the high incidence of lung cancer in this area and finding specific bio-molecular mechanisms involving the regional lung cancer.

Materials And Methods

Ethical statement

The experimental protocols were approved by the Ethics Committee of The Third Affiliated Hospital of Kunming Medical University, and performed according to the guidelines of the 1975 Declaration of

Helsinki. All participants involved in this study provided written informed consent.

Specimen collection

Total 20 lung cancer tissues and 20 adjacent normal lung tissues were collected from The Third Affiliated Hospital of Kunming Medical University. All subjects were born and lived in Xuanwei area for more than 3 generations, and with local bituminous coal contact history over 10 years. The pathologic diagnosis of each specimen was evaluated by a pathologist. None of the patients had received anti-tumor treatment before collecting specimens. The clinic pathological features were obtained from the medical records of lung cancer patients. All tissue specimens were stored at − 80 °C until use.

Cell culture

The lung cancer cell lines, A549 and NCI-H1299, were purchased from Shanghai Cellular Research Institute (Shanghai, China) and maintained in RPMI-1640 medium (ScienCell, Carlsbad, CA, USA) supplemented with 10% fetal bovine serum, 100 U/ml penicillin, 100 μg/ml streptomycin in a humidified incubator at 37C with 5% CO_2.

Western blotting

The cells were treated under the indicated conditions, and then lysed with RIPA buffer at pH 8.0 (150 mM NaCl, 50 mM Tris, 1% Triton X-100, 0.5% sodium deoxycholate, 0.1% SDS). All the samples were quantified using Pierce™ bicinchoninic acid (BCA) assay (Thermo Fisher Scientific Inc., IL, USA) to ensure equal loading of proteins. The cellular protein samples were subjected to SDS-PAGE, and then transferred to a polyvinylidene difluoride membrane (Millipore, Billerica, MA, USA). After blocked with 5% BSA, the membrane was probed with the primary antibody, then incubated with HRP-conjugated secondary antibody in TBST. β-actin was used as a loading control. Proteins were visualized using an enhanced chemiluminescence solution.

Cell Viability Assay

Cell viability was determined using CCK-8 assay (Beyotime, China) following the manufacturer's instruction.

ROS assay

For assay of ROS, the superoxide indicator dihydroethidium (DHE, Invitrogen) was added at 5 μM into cell culture medium and incubate for 1 h at 37 °C. Fluorescence was measured according to kit instructions with 485 nm excitation and 527 nm emission.

Malondialdehyde (MDA) assay

Levels of MDA, a product of lipid peroxidation, were measured based on reaction between MDA and thiobarbituric acid with commercial kit from Beyotime Biotechnology (Shanghai, China) [18]. The

enzymatic activities were recorded as units per milligram of protein (U/mg protein). Values obtained were the average of three independent measurements.

Animal Experiments

All animal experiments strictly adhered to local regulations as well as LAWER (Laboratory Animal Welfare Ethics Review) guidelines (Andersen and Winter, 2017; Herrmann and Flecknell, 2018), and were approved by the local authorities before initiation.

1×10^6 the indicated tumor cells in 100 μl of PBS were injected into the back of BALB/c-nu mice. The tumor volume (tv) of BALB/c-nu mice were monitored every week. The tv was calculated using the following formula: $tv = ab^2/2$, where a is the length of the tumor, and b is the width. The tumors were separated after mice euthanizing.

High-performance liquid chromatography (HPLC) and mass spectrometry analysis

Each sample was subjected to trypsin digestion and TMT labeling. Subsequently, the digested samples were separated with a capillary HPLC system. The Q-Exactive mass spectrometer from Thermo Finnigan was used to perform data acquisition.

Samples were separated by Easy nLC system with EASY column (Thermo scientific, 10 cm × 75 μm, 3 μm C18). The column temperature was set at 25 °C and injection volume was 10 μL. The gradient elution of mobile phase was at a flow rate of 250 nL/min. The mobile phase consisted of 0.1% formic acid in water (mobile phase A) and 84% acetonitrile plus 0.1% formic acid in water (mobile phase B). The gradient elution procedure was as follows: phase B started from 0%, and then increased linearly to 35% at 50 min, and further increased to 100% at 55 min, then was held for 5 min. During the whole analysis, the samples were in an automatic 4 °C injector. The samples were analyzed randomly. QC samples were inserted into the sample queue to monitor and evaluated the stability of the equipment and the reliability of the raw data.

MS analysis was performed using a Q-Exactive mass spectrometer (Thermo Finnigan) with a nano ESI source and an orbitrap analyzer, operating in positive ion modes. The mass spectrometer recorded ions with a range of 300–1800 m/z. The dynamic exclusion duration was 40.0 s. Survey scans were acquired at a resolution of 70 000 at m/z 200, and the resolution for the HCD spectra was set to 17 500 at m/z 200. The normalized collision energy was 30 eV, and the under-fill ratio was defined as 0.1%. QC samples were checked at an interval of 7 samples to ensure stability during the whole sequence.

Data processing

Raw MS/MS spectra data were analyzed using Mascot (version 2.2, Matrix Science, London, U.K.). The search engine was set up to search the SWISS-PROT database. Scaffold Q+ (version Scaffold_4.4.5, Proteome Software, Inc., Portland, OR, United States) was used to quantify the TMT peptide. A threshold of ± 1.2-fold change with p value < 0.05 was considered as significant changes. Statistical procedure was

performed with the t test. Gene Ontology (GO) annotation, including biological processes (BP), cellular components (CC), and molecular functions (MF), of the identified proteins was implemented using BLAST2TO (version 2.5), and pathway enrichment analysis of the differentially-expressed proteins was by Kyoto Encyclopedia of Genes and Genomes (KEGG) automatic annotation server.

Transmission Electron Microscopy (TEM)

The cells were washed with precooled PBS (pH 7.4) and then post-fixed in phosphate-buffered glutaraldehyde (2.5%) and osmium tetroxide (1%). The samples were then cut and stained en bloc with 2% uranyl acetate (UA), dehydrated in a graded ethanol series, and embedded in an epoxy resin. Then, the sections (70–90 nm) were stained with UA and lead citrate. Ultrastructural images were captured with a transmission electron microscope (Hitachi HT7700, Tokyo, Japan).

Statistical analysis

SPSS 20.0 statistical software (SPSS, Chicago, IL, USA) was used for data analysis. The indexes were analyzed by one-way ANOVA. Differences were set as significant at $P < 0.05$.

Results

The scheme of the proteomic analysis was presented in **Fig. 1A**. A total of 11134 peptides in the clinic tissue samples were detected, which covers 3473 proteins; of these, 422 differentially-expressed proteins (fold-change > 1.2 or < 0.83 in comparison with the para-carcinoma tissues, $p < 0.05$) were found in the analysis with quantitative information and were included in the next bioinformatics analysis. A volcano chart was drawn according to two factors, the fold-change and the p value obtained by t-test, to show the significant difference in data between the two groups of samples (Fig. 1**B**). We used the hierarchical cluster to compare the differentially expressed proteins of the representative cases, showing with the heat map (Fig. 1**C**). The chart indicated that the threshold of fold-change set in the current study can effectively separate the cancer and the para-carcinoma groups, and the data of each case from the two groups were reproducible. According to the description about in GO terms and several recently published studies, various proteins, including TXN2, HP, PCNA, MYH7, POLG, TMEM62, TMEM16F, TMEM131L, SLC34A2, SLC35A3, SLC9A3R2, SLC44A2, HSPH1, HSPA5, LPCAT1, PPP1R14A, PPP2R5C, were screened out (Fig. 1**D**), and subsequently subjected to qPCR validation (Fig. 1**E**).

The 422 proteins (162 upregulated and 260 downregulated versus para-carcinoma tissues) were annotated according to their biological process, cellular component, and molecular function by BLAST2TO (Fig. 2**A**). Biological processes analysis showed that these proteins were mainly involved in single-organism process, localization, cellular component organization or biogenesis, biological regulation, and multicellular organismal process. Cellular component analysis showed that most of the differential proteins were located in the extracellular region, membrane-enclosed lumen, and organelle. Molecular function analysis revealed that a large proportion of these proteins played a role in molecular function regulator, structural molecule activity, protein binding, transporter activity, and molecular

transducer activity. Pathway annotation by KEGG analysis demonstrated that these differential proteins are mainly involved in ECM-receptor interaction, focal adhesion, small cell lung cancer, PI3K/AKT pathway, and amoebiasis (Fig. 2**B**). The above pathways might be involved in the lung cancer in this area.

TXN2 and HP were relatively in the center of the PPI network of all DEPs, implying some important roles that they might play in the progression of NSCLC (red arrow, **Fig. 3A**). Other various ferroptosis-related proteins that were indicated with blue arrows (Fig. 3**A**) were scattered on the network, further suggesting that ferroptosis probably involved in the progression of NSCLC. In addition, we picked out TXN2 and HP to analyze more potential association with other possible molecules in ferroptosis (Fig. 3**B** and **3C**), and we noticed GPX4 (blue arrow), which is a documented key negative regulator of ferroptosis, and APOE (blue arrow), a well-known lipid peroxidation inhibitor, are closely implicated. In addition, we noticed that there are few studies about these two proteins TXN2 and HP in ferroptosis. Based on these findings, we decided to pay more attention on these two molecules in the following research.

We validated the changes of TXN2 and HP in proteomics using several lung cancer cell lines and clinic samples (Fig. 4**A** and **4B**). We next treated the cell lines with ferroptosis inducer, erastin, RSL, or sorafenib, and their effects on cells were verified with cell survival and MDA assays in **Supplementary Fig. 1 (Figure S1)**. We observed that TXN2 was significantly decreased but HP increased in the cells treated with the inducer at both mRNA and protein levels (Fig. 4**C** and **4D**), which indicated that the trend in proteomic analysis was reversed by the inducer. We hypotheses that regulating the levels of TXN2 and HP in lung cancer cells would influence the cell proneness to ferroptosis.

Using the online tool DriverDBv3 (http://driverdb.tms.cmu.edu.tw/), whose data source is TCGA, TXN2 expression was found enhanced in LUSC (lung squamous cell carcinoma) but not in LUAD (lung adenocarcinoma), compared to lung normal tissue (Fig. 5**A** and **5B**). To further explore the possible role of TXN2 in tumor progression of NSCLC, TXN2 expression in NSCLC from GEO public repository was analyzed with GENT2 (http://gent2.appex.kr/gent2/). As a result, we found higher TXN2 levels at later clinical stages, though it was lower in at some stages (Fig. 5**C**). If overexpressed TXN2 plays a role in progression of NSCLC, the patients with different TXN2 level may have different survival results. According to the survival analysis results from Kaplan Meier-plotter (http://kmplot.com/analysis/), high-TXN2-expression patients' overall survival time is shorter than that of low-expression NSCLC patients, especially for LUAD (Fig. 5**D** and **5E**). In one of the above datasets (GSE31210, analyzed with PrognoScan, http://dna00.bio.kyutech.ac.jp/PrognoScan/index.html), apart from the OS result consistent with that in Fig. 5D, TXN2-high-expression patients also exhibited lower RFS (relapse free survival) (Fig. 5**F** and **5G**). But for LUSC, no significantly differences were found between low-TXN2 and high-TXN2 groups (data not shown).

HP expression data in LUAD and LUSC from TCGA were analyzed with online tool DriverDBv3 (http://driverdb.tms.cmu.edu.tw/), and it was found that HP was notably downregulated in both LUAD and LUSC tissues, compared to lung normal tissue (Fig. 6**A** and **6B**). The possible role of HP in tumor

progression of NSCLC was revealed through analysis of its expression in NSCLC using GENT2 (http://gent2.appex.kr/gent2/) based on GEO public repository. However, lower HP at later clinical stages was not frequently observed (Fig. 6**C**). According to the survival analysis results from The Human Protein Atlas (https://www.proteinatlas.org/), low-HP-expression patients have a poorer overall survival in LUAD, but quite in reverse, low-HP-expression patients have a better prognosis for LUSC (Fig. 6**D** and **6E**). To further validate the role of HP in prognosis of NSCLC, we analyzed the survival of patients with low or high HP expression using Kaplan Meier-plotter (http://kmplot.com/analysis/) that mainly contains GEO (gene expression omnibus) datasets. Against our prediction and the aforesaid result from TCGA, the low-HP-expression patients' overall survival was better, consistent with which, these patients showed longer time till first progression (Fig. 6**F** and **6G**). In addition, according the survival analysis results from GEO datasets, HP expression level showed no effect on LUSC patients' survival (data not shown).

Then we over-expressed HP or interfered with TXN2 in lung cancer cell lines, and observed that the transfected cells became more prone to erastin or RSL-induced ferroptosis compared to non-transfected cells by showing lower rates of survival (Fig. 7**A**). MDA assays indicated the lower oxidative metabolism of lipids in the blank lung cancer cells under the erastin or RSL treatment, while the transfected cells had an increased the levels of membrane lipid oxidation (Fig. 7**B**). Similarly, changes in ROS also indicated a significant increase in oxidation levels of the transfected cells under erastin or RSL treatment (Fig. 7**C**). The GSH assays showed that the GSH in the transfected cells was almost exhausted (Fig. 7**D**). Observation by TEM revealed that the lung cancer cells with interference of TXN2 or overexpression of HP had smaller mitochondria and a decreased number of mitochondrial cristae under the treatment of erastin or RSL, and the proportion of mitochondria with ruptured outer membrane increased in these cells (Fig. 7**E**). These results suggested that upregulating of HP but downregulating TXN2 can increase the ferroptosis rate of lung cancer cells.

Afterwards, we constructed the siTXN2 but HP overexpressing A549 cell, and performed the tumorigenicity tests using the wild type A549 and the cotransfected A549 cells on nude mice. We found that the cotransfected cell was more sensitive to erastin or RSL treatment in vivo, which showed that the tumor volume was much smaller than the group of wild type A549 at 28 days after implantation (Fig. 8). Therefore, promoting the development of lung cancer by inhibiting ferroptosis may be a potential and special mechanism for the high incidence of lung cancer in Xuanwei.

Discussion

Ferroptosis is a recently identified form of cell death, which differs from apoptosis, cell necrosis, and autophagy. It is caused by the accumulation of the products of iron-dependent lipid peroxidation (16, 17). This type of cell death was named by Dixon in 2012. Morphologically, the cells showed a decrease in volume, an increase in mitochondrial membrane density, and disappearance of mitochondrial cristae during ferroptosis (18). At the molecular level, ferroptosis is manifested by the inhibition of the activity of phospholipid glutathione peroxidase 4 (GPX4), which in turn results in the accumulation of the products of lipid peroxidation involved by iron elements in cells (19). Aberrances in ferroptosis are associated with

the occurrence of various diseases, such as ischemia-reperfusion injury of organs (20), tumors (21) and stroke (22). Several molecular pathways have been found to be involved in the process of ferroptosis, such as the RAS/MAPK (23) and NRF2 pathways (24). However, many specific mechanisms and regulatory factors of ferroptosis are not fully understood.

Iron is the most abundant metal element in the human body. It is mainly used in vivo as a cofactor for proteins, such as hemoglobin and various enzymes. The survival of all independent life forms requires iron on Earth (25). However, excess iron is related to the occurrence of various diseases because iron catalyzes many oxidative reactions, which generates a lot of free radicals and increases oxidative stress in the body (26, 27). Biomolecules containing active thiol groups are necessary to maintain redox balance, normal metabolism and detoxification in living organisms. As an important active thiol-containing substance in the body, thioredoxin has attracted researchers' attention to its role in ferroptosis (28). Ferroptosis was observed in cancer and cancer stem cells. Excess iron in the presence of oxygen appears the most commonly known mutagen. The persistent activation of antioxidant systems and overexpression of thioredoxin via genetic alterations in Nrf2 and Keap1 also contributes to carcinogenesis (29). A recent study reported that a diterpene natural product pleuromutilin was subjected to reaction sequences, which resulted in a collection of compounds with previously unreported ring systems, providing a novel set of structurally diverse and highly complex compounds suitable for screening, and then biological evaluation identified the novel compound ferroptocide, a small molecule that rapidly and robustly induces ferroptotic death of cancer cells. Further target identification efforts revealed that ferroptocide was an inhibitor of thioredoxin (30). Thus, the ferroptocide due to its inhibiting role for thioredoxin would be a useful tool to study the utility of pro-ferroptotic agents for treatment of cancer.

Haptoglobin combines with free plasma hemoglobin to allow hepatic recycling of heme iron and to prevent kidney damage. Haptoglobin also has antibacterial activity, and plays a role in modulating many aspects of the acute phase response (31). Hemoglobin/haptoglobin complexes are rapidly cleared by the macrophage CD163 scavenger receptor expressed on the surface of liver Kupfer cells through an endocytic lysosomal degradation pathway (32). The expression of HP was found increased after Intracerebral hemorrhage *in vivo*, which could prevent hemoglobin-induced neuronal ferroptosis as an antioxidant (33).

The Xuanwei area in Yunnan Province is the main coal mining area in southwestern China, and it is also a high-risk area for lung cancer. Several geochemical studies have shown that mineral elements in this area are associated with a high incidence of lung cancer in the area (10, 34). Considering iron is the main chemical element in the particles emitted from Xuanwei coal combustion, and reactive oxygen species (ROS) could be generated by redox-active transition metals (TM) in particles, a study focused on the valence state of iron in size-resolved particle found that a large fraction of oxidizable iron could be found in raw coal samples, and the acid extractable, reducible and oxidizable fractions of iron in the fly ash particles accounted for a large proportion (46%-78%) in the size-resolved particles after coal combustion. In addition, The concentration of ·OH was higher in fine particles than coarse particles (35).

Herein we analyzed the protein profiling of the lung cancer tissues from clinic patients of Xuanwei area, and found that ECM-receptor interaction, focal adhesion, and PI3K/AKT pathway may involve in the development of the lung cancer. In addition, the results also indicated ferroptosis-related molecules, TXN2 and HP, also significantly changed. Further experiments demonstrated that the changes of the TXN2 and HP expressions made the cancer cells more resistant to erastin or RSL-induced cell death, which could be a specific mechanism for the lung cancer in Xuanwei area. Further studies are needed to verify the changes in a larger cohort and to establish the association between the molecules and the high incidence of lung cancer in Xuanwei area.

Declarations

Data Availability Statement

The data that supports the findings of this study are available in the manuscript and supplementary materials.

Acknowledgements: This study was supported by National Natural Science Foundation of China (Nos.: 81960500, 81702274); National Key Research and Development Program (Nos.: 2017YFC0907902, 2016YFE0103400); Yunnan Fundamental Research Projects (Nos.: 2017FE467(-187), 2018FE001(-152), and 2017FE468(-159)); Yunnan Health Training Project of Leading Scholars (No.: D2017012); Internal Organization Research Projects of Yunnan Cancer Hospital (No.: 2017NS199). The funders had no role in study design, data collection and analysis, decision to publish, or preparation of the manuscript.

Conflict of Interest: The authors declare no potential conflict of interest.

Author contributions statement: GJL and JPY performed the experiments and collected the data; they were major contributors in writing the manuscript, and they were co-first authors. GQZ, ZHS, KYY, LWT, RWP and QHZ were responsible for data analysis and visualization. YC and ZY conceived and designed the study, and they were major contributors in critically revising the manuscript. All authors read and approved the final manuscript.

References

1. Navarro Silvera SA, Rohan TE. Trace elements and cancer risk: a review of the epidemiologic evidence. Cancer Causes Control. 2007;18(1):7–27. doi:10.1007/s10552-006-0057-z.
2. Mumford JL, He XZ, Chapman RS, Cao SR, Harris DB, Li XM,.. . et al. Lung cancer and indoor air pollution in Xuan Wei, China. Science. 1987;235(4785):217–20. doi:10.1126/science.3798109.
3. Zhang L, Lv J, Liao C. Dietary exposure estimates of 14 trace elements in Xuanwei and Fuyuan, two high lung cancer incidence areas in China. Biol Trace Elem Res. 2012;146(3):287–92. doi:10.1007/s12011-011-9252-1.

4. Lan Q, He X, Shen M, Tian L, Liu LZ, Lai H,.. . Chapman RS. Variation in lung cancer risk by smoky coal subtype in Xuanwei, China. Int J Cancer. 2008;123(9):2164–9. doi:10.1002/ijc.23748.
5. Zhang L, Li J, Wang Y, Wu G, Wei F. [Descriptive study of the environmental epidemiology of high lung cancerincidence rate in Qujing, Yunnan, China]. Zhongguo Fei Ai Za Zhi. 2012;15(3):159–63. doi:10.3779/j.issn.1009-3419.2012.03.05.
6. Large DJ, Kelly S, Spiro B, Tian L, Shao L, Finkelman R,.. . Zhou Y. Silica-volatile interaction and the geological cause of the Xuan Wei lung cancer epidemic. Environ Sci Technol. 2009;43(23):9016–21. doi:10.1021/es902033j.
7. Baan R, Grosse Y, Straif K, Secretan B, El Ghissassi F, Bouvard V,.. . Group WH. O. I. A. f. R. o. C. M. W. (2009). A review of human carcinogens–Part F: chemical agents and related occupations. Lancet Oncol, 10(12), 1143–1144. doi:10.1016/s1470-2045(09)70358-4.
8. Straif K, Benbrahim-Tallaa L, Baan R, Grosse Y, Secretan B, Ghissassi E, Group F. W. H. O. I. A. f. R. o. C. M. W. (2009). A review of human carcinogens–Part C: metals, arsenic, dusts, and fibres. Lancet Oncol, 10(5), 453–454. doi:10.1016/s1470-2045(09)70134-2.
9. Lan Q, Chapman RS, Schreinemachers DM, Tian L, He X. Household stove improvement and risk of lung cancer in Xuanwei, China. J Natl Cancer Inst. 2002;94(11):826–35. doi:10.1093/jnci/94.11.826.
10. Zhang WC, Lu SL, Liu DY, Liu PW, Yonmochi S, Wang XJ, Wang QY. (2015). [Distribution Characteristics of Heavy Metals in the Street Dusts in Xuanwei and Their Health Risk Assessment]. Huan Jing Ke Xue, 36(5), 1810–1817. Retrieved from https://www.ncbi.nlm.nih.gov/pubmed/26314134.
11. Attafi IM, Bakheet SA, Korashy HM. The role of NF-kappaB and AhR transcription factors in lead-induced lung toxicity in human lung cancer A549 cells. Toxicol Mech Methods. 2020;30(3):197–207. doi:10.1080/15376516.2019.1687629.
12. Chen QY, Murphy A, Sun H, Costa M. Molecular and epigenetic mechanisms of Cr(VI)-induced carcinogenesis. Toxicol Appl Pharmacol. 2019;377:114636. doi:10.1016/j.taap.2019.114636.
13. Chen W, Fu W, Deng Q, Li Y, Wang K, Bai Y,.. . Guo H. Multiple metals exposure and chromosome damage: Exploring the mediation effects of microRNAs and their potentials in lung carcinogenesis. Environ Int. 2019;122:291–300. doi:10.1016/j.envint.2018.11.020.
14. Lv J, Zhang W, Xu R. (2013). Investigation of radon and heavy metals in Xuanwei and Fuyuan, high lung cancer incidence areas in China. J Environ Health, 76(4), 32–38. Retrieved from https://www.ncbi.nlm.nih.gov/pubmed/24341159.
15. Tan Z, Lu S, Zhao H, Kai X, Jiaxian P, Win MS,.. . Wang Q. Magnetic, geochemical characterization and health risk assessment of road dust in Xuanwei and Fuyuan, China. Environ Geochem Health. 2018;40(4):1541–55. doi:10.1007/s10653-018-0070-7.
16. Dixon SJ, Lemberg KM, Lamprecht MR, Skouta R, Zaitsev EM, Gleason CE,.. . Stockwell BR. Ferroptosis: an iron-dependent form of nonapoptotic cell death. Cell. 2012;149(5):1060–72. doi:10.1016/j.cell.2012.03.042.

17. Xie Y, Hou W, Song X, Yu Y, Huang J, Sun X,.. . Tang D. Ferroptosis: process and function. Cell Death Differ. 2016;23(3):369–79. doi:10.1038/cdd.2015.158.
18. Nguyen THP, Mahalakshmi B, Velmurugan BK. Functional role of ferroptosis on cancers, activation and deactivation by various therapeutic candidates-an update. Chem Biol Interact. 2020;317:108930. doi:10.1016/j.cbi.2019.108930.
19. Shi ZZ, Fan ZW, Chen YX, Xie XF, Jiang W, Wang WJ,.. . Bai J. Ferroptosis in Carcinoma: Regulatory Mechanisms and New Method for Cancer Therapy. Onco Targets Ther. 2019;12:11291–304. doi:10.2147/OTT.S232852.
20. Friedmann Angeli JP, Schneider M, Proneth B, Tyurina YY, Tyurin VA, Hammond VJ,.. . Conrad M. Inactivation of the ferroptosis regulator Gpx4 triggers acute renal failure in mice. Nat Cell Biol. 2014;16(12):1180–91. doi:10.1038/ncb3064.
21. Shen Z, Song J, Yung BC, Zhou Z, Wu A, Chen X. Emerging Strategies of Cancer Therapy Based on Ferroptosis. Adv Mater. 2018;30(12):e1704007. doi:10.1002/adma.201704007.
22. Alim I, Caulfield JT, Chen Y, Swarup V, Geschwind DH, Ivanova E,.. . Ratan RR. Selenium Drives a Transcriptional Adaptive Program to Block Ferroptosis and Treat Stroke. Cell. 2019;177(5):1262–79 e1225. doi:10.1016/j.cell.2019.03.032.
23. Yagoda N, von Rechenberg M, Zaganjor E, Bauer AJ, Yang WS, Fridman DJ,.. . Stockwell BR. RAS-RAF-MEK-dependent oxidative cell death involving voltage-dependent anion channels. Nature. 2007;447(7146):864–8. doi:10.1038/nature05859.
24. Sun X, Ou Z, Chen R, Niu X, Chen D, Kang R, Tang D. Activation of the p62-Keap1-NRF2 pathway protects against ferroptosis in hepatocellular carcinoma cells. Hepatology. 2016;63(1):173–84. doi:10.1002/hep.28251.
25. Toyokuni S. Iron and thiols as two major players in carcinogenesis: friends or foes? Front Pharmacol. 2014;5:200. doi:10.3389/fphar.2014.00200.
26. Agudo A, Bonet C, Sala N, Munoz X, Aranda N, Fonseca-Nunes A,.. . Jakszyn P. Hemochromatosis (HFE) gene mutations and risk of gastric cancer in the European Prospective Investigation into Cancer and Nutrition (EPIC) study. Carcinogenesis. 2013;34(6):1244–50. doi:10.1093/carcin/bgt045.
27. Fracanzani AL, Conte D, Fraquelli M, Taioli E, Mattioli M, Losco A, Fargion S. Increased cancer risk in a cohort of 230 patients with hereditary hemochromatosis in comparison to matched control patients with non-iron-related chronic liver disease. Hepatology. 2001;33(3):647–51. doi:10.1053/jhep.2001.22506.
28. Lu J, Holmgren A. The thioredoxin antioxidant system. Free Radic Biol Med. 2014;66:75–87. doi:10.1016/j.freeradbiomed.2013.07.036.
29. Mitsuishi Y, Motohashi H, Yamamoto M. The Keap1-Nrf2 system in cancers: stress response and anabolic metabolism. Front Oncol. 2012;2:200. doi:10.3389/fonc.2012.00200.
30. Llabani E, Hicklin RW, Lee HY, Motika SE, Crawford LA, Weerapana E, Hergenrother PJ. Diverse compounds from pleuromutilin lead to a thioredoxin inhibitor and inducer of ferroptosis. Nat Chem. 2019;11(6):521–32. doi:10.1038/s41557-019-0261-6.

31. Fasano A. Zonulin and its regulation of intestinal barrier function: the biological door to inflammation, autoimmunity, and cancer. Physiol Rev. 2011;91(1):151–75. doi:10.1152/physrev.00003.2008.
32. Galea J, Cruickshank G, Teeling JL, Boche D, Garland P, Perry VH, Galea I. The intrathecal CD163-haptoglobin-hemoglobin scavenging system in subarachnoid hemorrhage. J Neurochem. 2012;121(5):785–92. doi:10.1111/j.1471-4159.2012.07716.x.
33. Zhao X, Song S, Sun G, Strong R, Zhang J, Grotta JC, Aronowski J. Neuroprotective role of haptoglobin after intracerebral hemorrhage. J Neurosci. 2009;29(50):15819–27. doi:10.1523/JNEUROSCI.3776-09.2009.
34. Coyle YM, Minahjuddin AT, Hynan LS, Minna JD. (2006). An ecological study of the association of metal air pollutants with lung cancer incidence in Texas. J Thorac Oncol, 1(7), 654–661. Retrieved from https://www.ncbi.nlm.nih.gov/pubmed/17409932.
35. Wang QX, Tan ZY, Zhao H, Li JH, Tian LW, Wang QY,.. . Lu SL. [Species of Iron in Size-resolved Particle Emitted from Xuanwei Coal Combustion and Their Oxidative Potential]. Huan Jing Ke Xue. 2017;38(6):2273–9. doi:10.13227/j.hjkx.201611110.

Figures

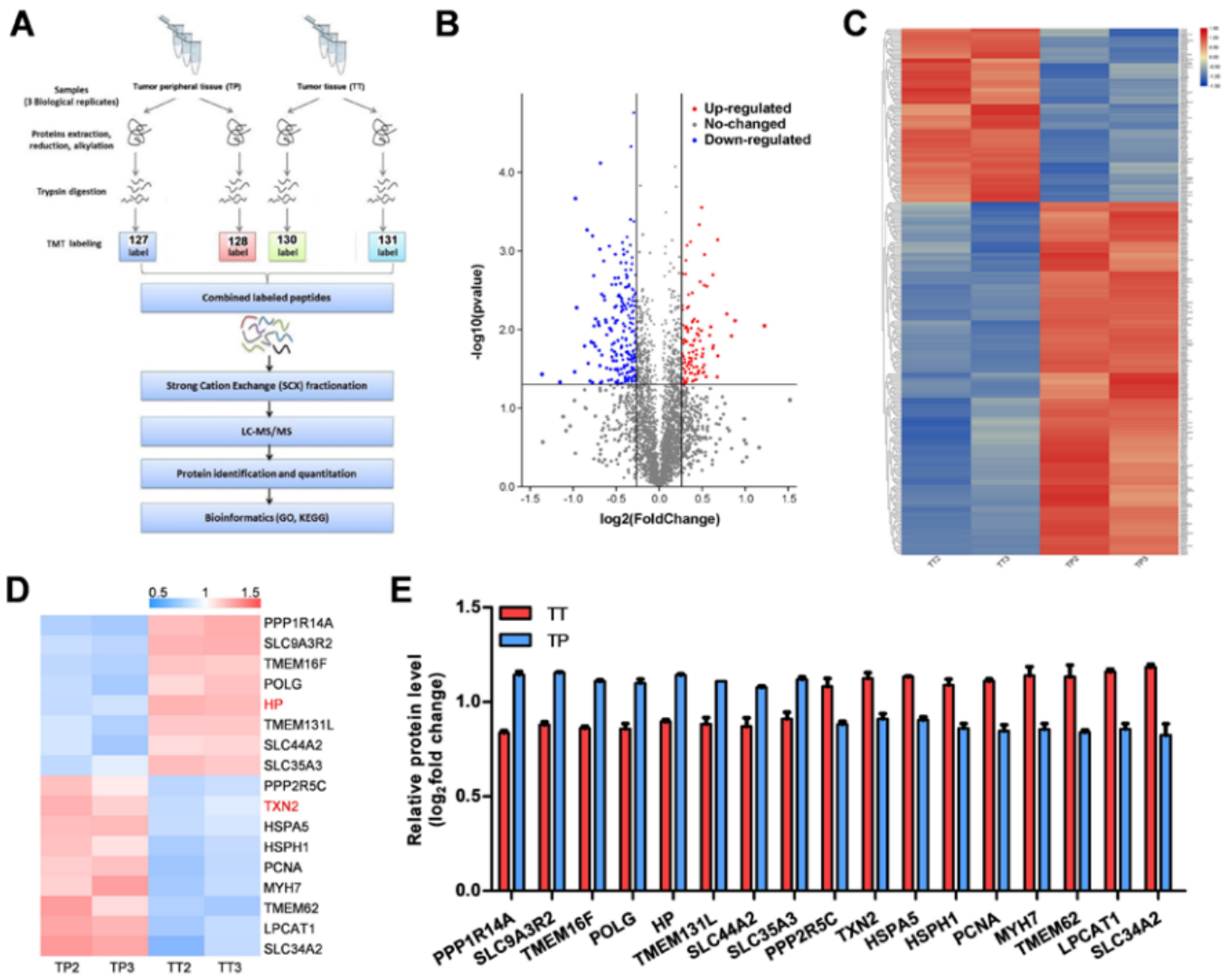

Figure 1

The proteomic analysis for the clinic carcinoma and para-carcinoma tissues of the patients diagnosed as lung cancer in Xuanwei. (A) The scheme of the proteomic analysis in this study. (B) The volcano plot showed the differentially expressed genes in the clinic samples. (C) Hierarchical clustering of the differentially-expressed genes. For hierarchical clustering, blue and red indicate decreased and increased expression, respectively. The proteins were clustered by hierarchical clustering using the complete linkage algorithm and Pearson correlation metric in R. (D) Heatmap of the proteins potentially related to ferroptosis. (E) Relative protein level of the molecules potentially related to ferroptosis; data were collected from the proteomic analysis results.

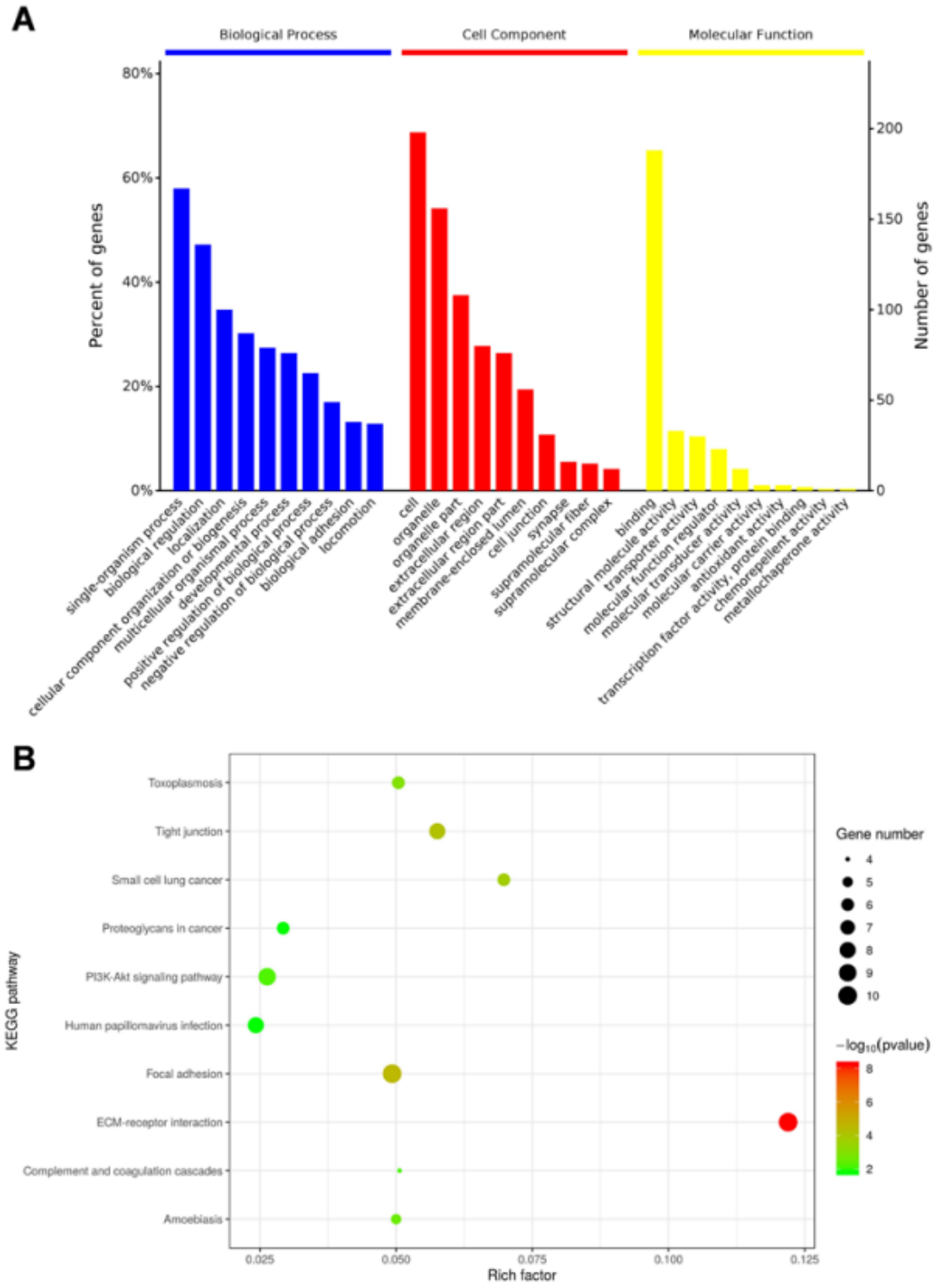

Figure 2

Bioinformatic analysis for the proteomic data. (A) GO classification of the differential proteins by biological process, cellular component, and molecular function. (B) KEGG analysis of the differential proteins. To the left of each plot: KEGG terms. Under each plot: the percentage of the sequence.

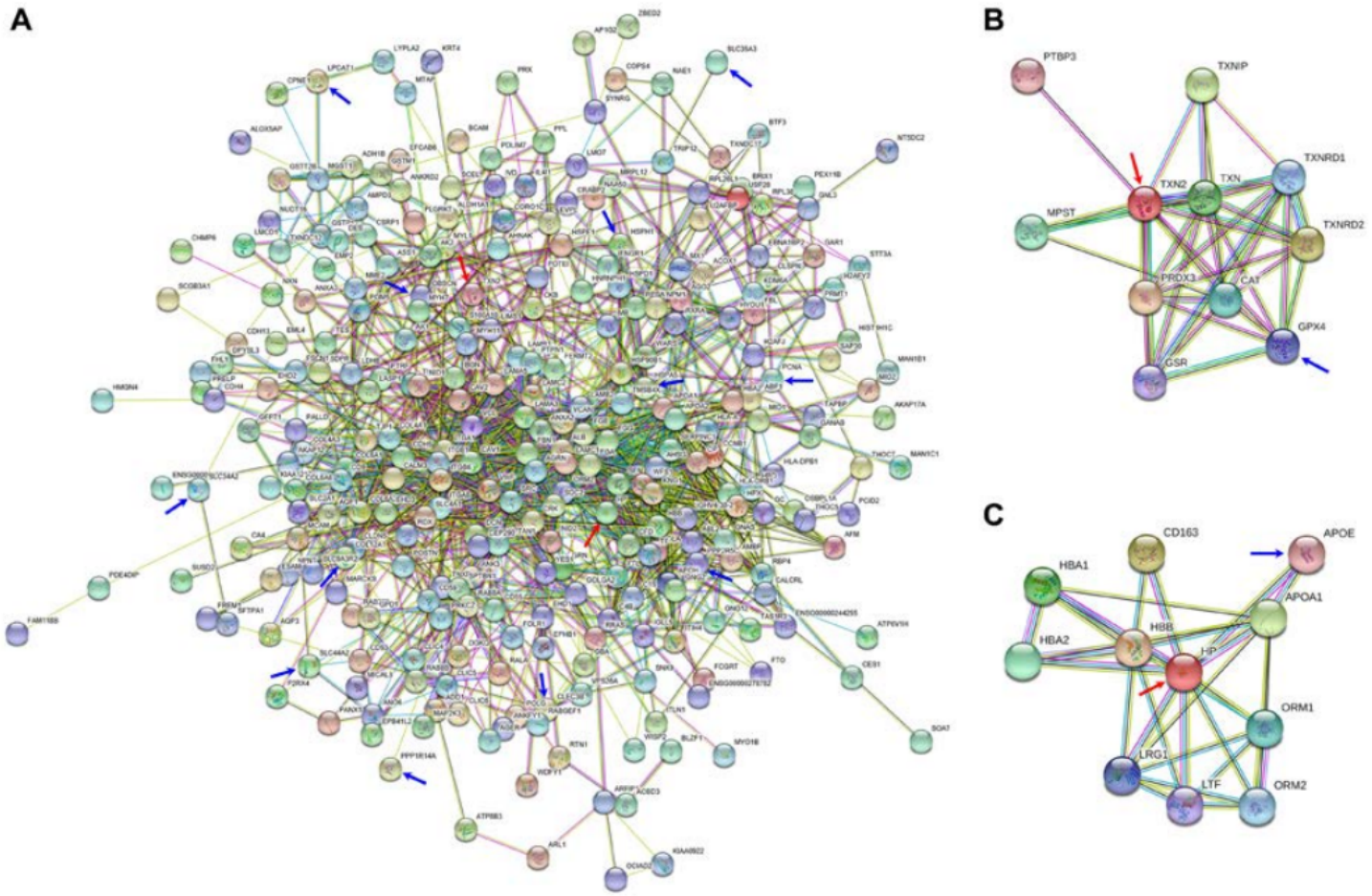

Figure 3

Protein-protein interaction (PPI) networks. A. PPI of all DEPs with a log2 (fold change) >1.2 or <0.83. The data were uploaded to the STRING 11.0 software to analyze the interactions among all DEPs. B. PPI network of TXN2-related proteins, including NDEPs and DEPs. C. PPI network of TXN2-related proteins, including NDEPs and DEPs. Colored ball: the changed protein; yellow line: text mining; purple line: experiments; blue line: databases; light blue: homology; black line: co-expression; green line: neighborhood; red line, gene fusion; deep blue: co-occurrence. DEPs: differentially expressed proteins; NDEPs: non-differentially expressed proteins.

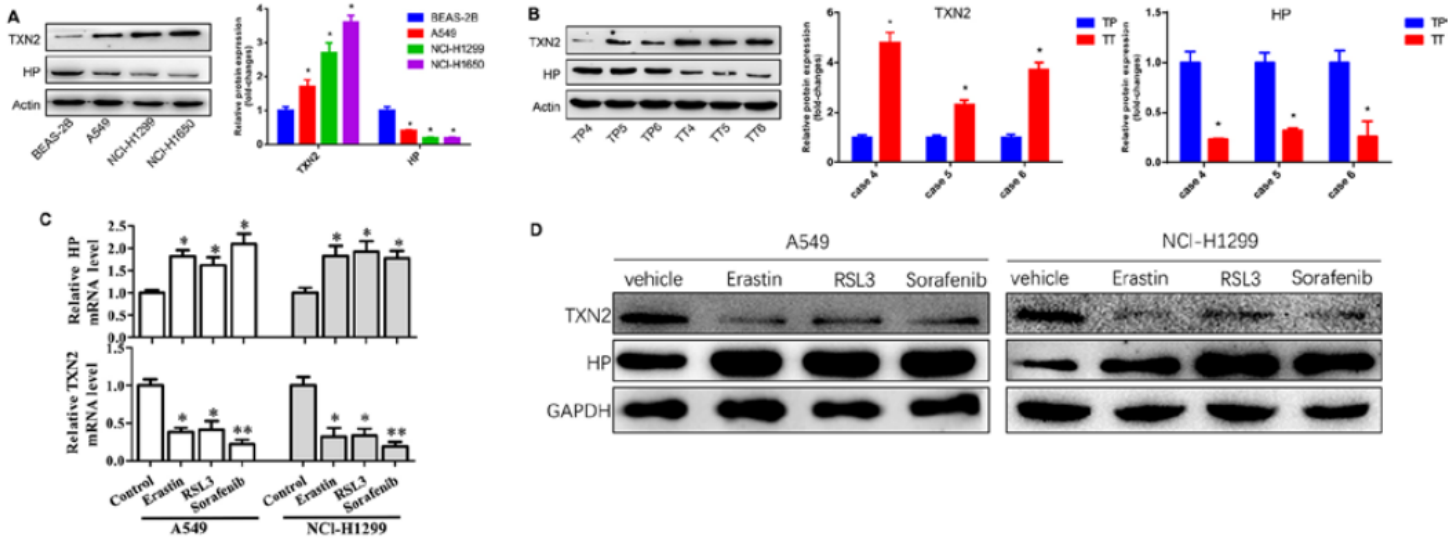

Figure 4

Validation of proteomics results. (A) Two differentially expressed proteins TXN2 and HP in lung cell lines were detected by Western blotting. *, $p < 0.05$. (B) The proteomics results of TXN2 and HP were validated in the clinic samples. TP, tumor peripheral tissue; TT, Tumor tissue. *, $p < 0.05$. (C) The expression of TXN2 and HP at mRNA level under the treatment of ferroptosis inducer, erastin (10 μM), RSL (1 μM) or sorafenib (5 μM). *, $p < 0.05$; **, $p < 0.01$. (D) The expression of TXN2 and HP at protein level under the treatment of ferroptosis inducer, erastin (10 μM), RSL (1 μM) or sorafenib (5 μM).

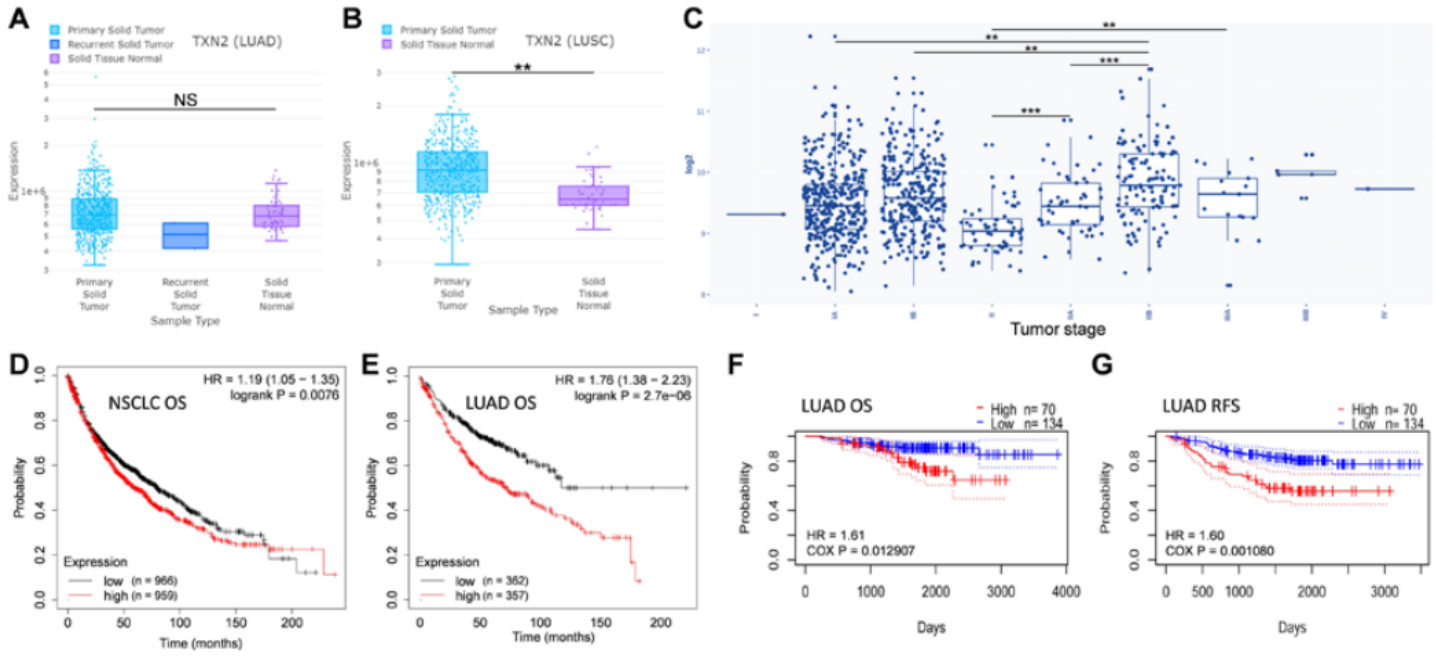

Figure 5

TXN2 expression profile in NSCLC and its role in prognosis. (A-B) TXN2 expression in LUAD (lung adenocarcinoma), LUSC (lung squamous cell carcinoma) and lung normal tissues. (C) TXN2 expression

in NSCLC, including LUAD, LUSC and LCLC (large cell lung cancer), from GEO public repository showed higher levels in at later clinical stages. (D-E) Overall survival analysis of TXN2-low and TXN2-high NSCLC (LUAD & LUSC; D) patients or LUAD patients (E); patients split by median; probe: 209078_s_at. (F-G) Overall survival and RFS (relapse free survival) analyses of TXN2-low and TXN2-high LUAD patients; probe: 209077_at.

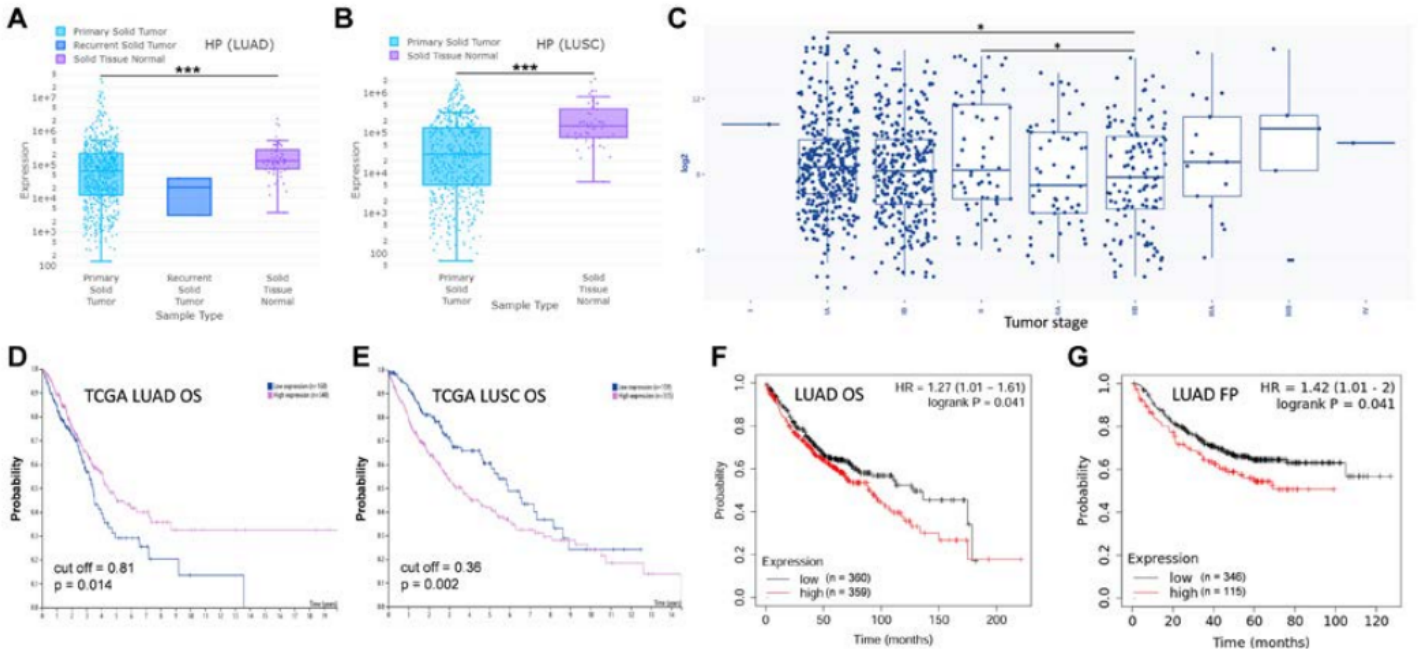

Figure 6

HP expression profile in NSCLC and its role in prognosis. (A-B) HP expression in LUAD, LUSC and lung normal tissues. (C) HP expression in NSCLC, including LUAD, LUSC and LCLC, from GEO public repository showed higher levels in at later clinical stages. (D-E) Overall survival analysis of HP-low and HP-high LUAD (D) or LUSC (E) patients. (F-G) Overall survival and FP (first progression) analyses of HP-low and HP-high LUAD patients; probe: 206697_s_at.

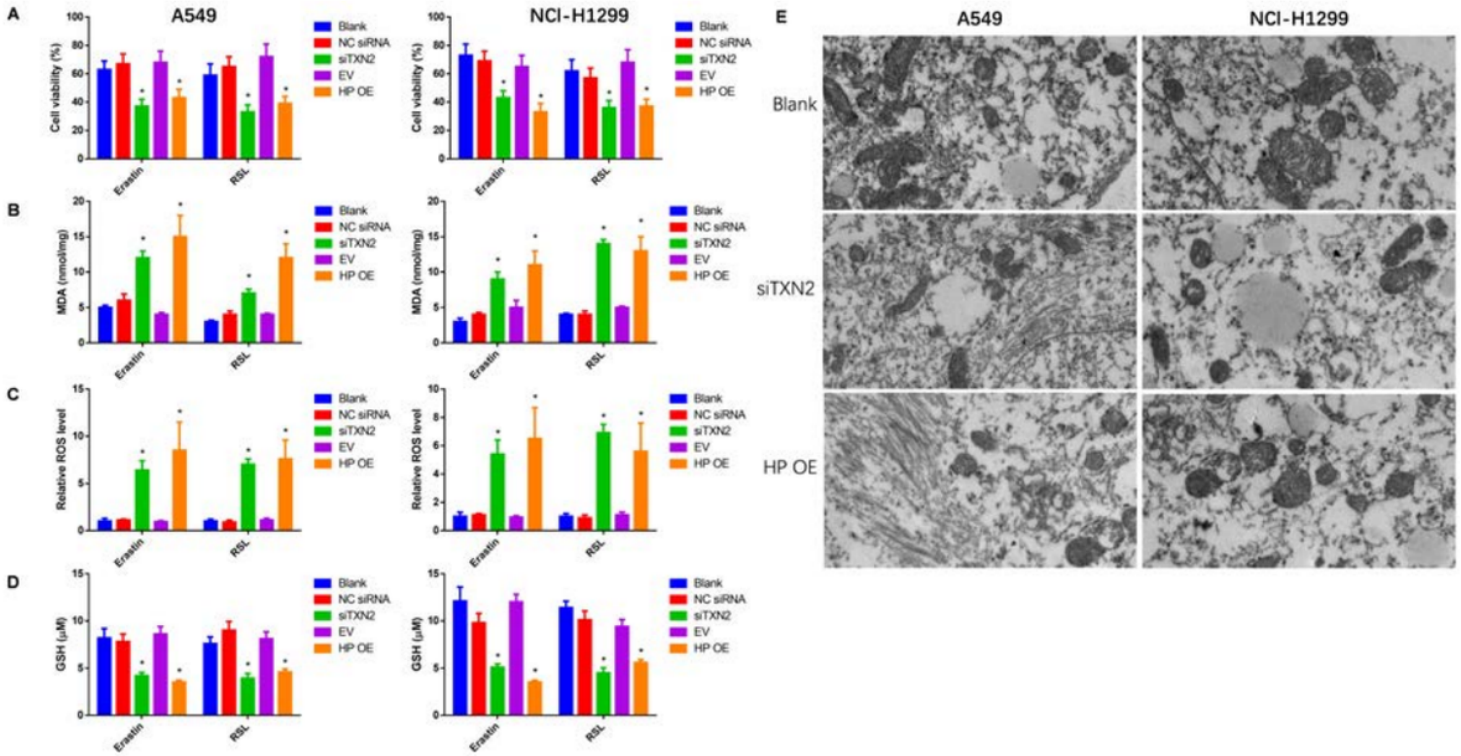

Figure 7

The expressions of TXN2 and HP affected ferroptosis in lung cancer cell lines A549 and NCI-H1299. (A) Cell viability assays for the cells under the treatment of erastin (10 μM) or RSL (1 μM) for 24 hours. (B) The MDA concentrations of the cells under the treatment of erastin (10 μM) or RSL (1 μM) for 24 hours. (C) The relative ROS levels in the cells under the treatment of erastin (10 μM) or RSL (1 μM) for 24 hours. (D) The GSH concentrations of the cells under the treatment of erastin (10 μM) or RSL (1 μM) for 24 hours. NC, negative control; EV, empty vector; OE, overexpressing; *, $p < 0.05$. (E) The alterations of mitochondrial ultrastructure of the indicated cells.

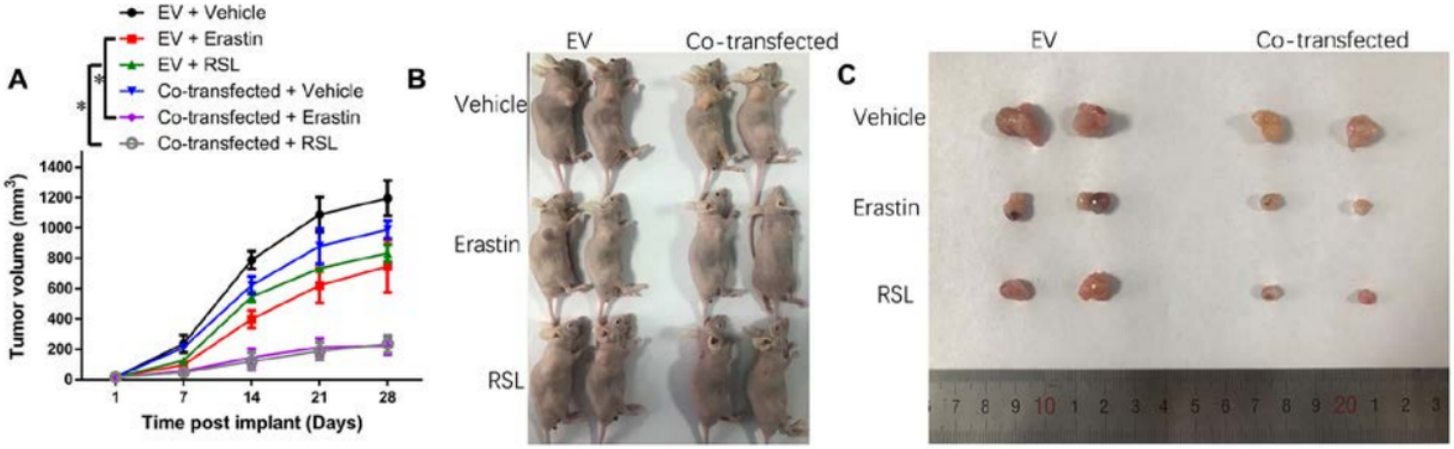

Figure 8

The expressions of TXN2 and HP affected ferroptosis in nude mice. (A) The tumor volume was monitored weekly. *, $p < 0.05$. (B-C) The tumor sizes at 28 days after implantation.

Supplementary Files

This is a list of supplementary files associated with this preprint. Click to download.

- figs1.png